Available online at www.sciencedirect.com
SCIENCE DIRECT®
Journal of Food Engineering 69 (2005) 41–49
JOURNAL OF FOOD ENGINEERING
www.elsevier.com/locate/jfoodeng

Development of a multi-spectral vision system for the detection of defects on apples

O. Kleynen *, V. Leemans, M.-F. Destain

Unité de Mécanique et Construction, Faculté Universitaire des Sciences Agronomiques de Gembloux, Passage des Déportés, 2, B-5030 Gembloux, Belgium

Received 12 February 2004; accepted 10 July 2004

Abstract

A method to sort 'Jonagold' apples based on the presence of defects was proposed. A multi-spectral vision system including four wavelength bands in the visible/NIR range was developed. Multi-spectral images of sound and defective fruits were acquired tending to cover the whole colour variability of this bicolour apple variety. Defects were grouped into four categories: slight defects, more serious defects, defects leading to the rejection of the fruit and recent bruises. Stem-ends/calyxes were detected using a correlation pattern matching algorithm. The efficiency of this method depended on the orientation of the stem-end/calyx according to the optical axis of the camera. Defect segmentation consisted in a pixel classification procedure based on the Bayes' theorem and non-parametric models of the sound and defective tissue. Fruit classification tests were performed in order to evaluate the efficiency of the proposed method. No error was made on rejected fruits and high classification rates were reached for apples presenting serious defects and recent bruises. Fruits with slight defects presented a more important misclassification rate but those errors fitted however the quality tolerances of the European standard. Considering an actual ratio of sound fruits of 90%, less than 2% of defective fruits were classified into the sound ones.

Keywords: Bicolour fruit; Pattern matching; Segmentation; Bayes' theorem; Classification; Sorting

1. Introduction

The marketing standard applying to apples in Europe is laid down by the EC Commission Regulation No 1619/2001. This standard defines three quality classes depending on the shape of the fruit, the colouring and the presence of defects. In Belgium, 'Jonagold' apples represent a large part (>60%) of the whole apple production. With regard to the presence of defects, the automatic grading of 'Jonagold' apples is still an arduous task because of the high natural variability of the skin colour of this bicolour apple variety.

Leemans and Destain (2004) presented a hierarchical method to grade 'Jonagold' apples using standard 3-CCD colour cameras. Colour images covering the whole surface of the fruit were acquired. These images were segmented on the basis of the Bayes' theorem. The probability distributions of the healthy tissue and the defects were considered as non-Gaussian and modelled numerically. The fruits were correctly graded with a rate of 73%. Errors came from a bad segmentation of the defects or from a confusion with the calyx and stem-ends. Defects badly segmented consisted essentially in russet and recent bruises which presented a colour similar to the healthy tissue (particularly it was difficult to distinguish russet in the transition area between the ground colour and the blush).

3-CCD colour cameras are not fully adapted to the defect detection of fruits since they are designed to

* Corresponding author. Tel.: +32 81 622165; fax: +32 81 622167.
E-mail address: kleynen.o@fsagx.ac.be (O. Kleynen).
URL: http://www.fsagx.ac.be/me/.

0260-8774/$ - see front matter © 2004 Elsevier Ltd. All rights reserved.
doi:10.1016/j.jfoodeng.2004.07.008

reproduce the human vision. Several methods based on more specific image acquisition methods are reported in the literature. Wen and Tao (1999) developed a near-infrared vision system for automating apple defect inspection. It was made of a monochrome CCD camera attached with a 700 nm long-pass filter. The inspection procedure consisted of a binary decision-tree-structured rule base that contained four process steps: blob extraction, feature extraction, rule base construction and recognition. Stem-ends and calyxes were separated from defects by means of the histogram density feature of the blob. Classification tests were performed on 960 samples of 'Red Delicious' apples. High recognition rates for good and defective apples could be achieved by setting proper parameters of the system. However, russet defects had a low recognition rate because the infrared vision system was not sensitive in the visible region. The tests also showed that light scars presented a high error rate and that stem-end/calyx recognition should be improved. In order to address the stem-end/calyx recognition problem, Cheng, Tao, Chen, and Luo (2003) proposed a near-infrared (NIR) and a mid-infrared (MIR) dual-camera vision system. The NIR and MIR cameras had, respectively, a sensitive spectrum range from 700 to 750 nm and from 7.5 to 13.5 μm. The NIR camera could identify both the stem-end/calyx portion of the apple and the true defects, while MIR camera could detect only the stem-ends and calyxes on refrigerated fruits. After initial pre-processing, NIR and MIR images were separately segmented based on the grey level similarity of the fruit pixels. The similarity was evaluated with an Euclidean distance. In NIR images, apple pixels were segmented into non-defective and defective groups. In MIR images, pixels were segmented into stem-ends/calyxes and other portions of the fruit. Then, segmented NIR and MIR images were compared to remove stem-ends and calyxes from true defects. Recognition tests were performed on 155 refrigerated 'Red Delicious' apples. Recognition rates of about 94% for stem-ends and 92% for calyxes were achieved. The correct classification rates of good and defective apples were, respectively, 100% and 92%. Shahin, Tollner, McClendon, and Arabnia (2002) used a line-scan X-ray imaging device to detect bruises in 'Red Delicious' and 'Golden Delicious' apples. New (24 h) and old (1 month) bruises were analysed. A set of spatial and transform features were tested. Classification tests were performed and best results were obtained using an artificial neural network and two kinds of features: spatial edge features and discrete cosine transform coefficients. For old bruises, an accuracy of 90% and 93% was achieved, respectively, for 'Red Delicious' and 'Golden Delicious' apples. New bruises were not adequately separated using this methodology (accuracy was approximately 60% for both apple varieties). Li, Wang, and Gu (2002) developed an automated apple surface defect sorting system based on monochromatic cameras equipped with interference bandpass filters centred at 840 nm. Defects were segmented by sub-tracting the original fruit image from a reference sound apple image. Then stem-ends and calyxes were separated from defects by using fractal features and artificial neural network. The method was tested on forty samples of 'Fuji' apples. Defects and stem-ends/calyxes were visually well segmented from the sound part of the fruit but no classification rates were provided. Regarding the stem-end/calyx recognition, the accuracy of the neural network classifier was over 93%. The authors did not precise if this result was obtained during the training process or in validation. Mehl, Chen, Kim, and Chan (2004) used an hyper-spectral imaging system for selecting a reduced number of wavelength to detect defects on the surface of 'Red Delicious', 'Golden Delicious', 'Gala' and 'Fuji' apples. They worked on five sound and five defective fruits of each cultivar. An asymmetric second difference method using a chlorophyll absorption wavelength at 685 nm and two wavelengths in the near-infrared band was found to provide the best visual separation of defective parts from the sound parts of the apples.

From these studies, it appears that apple defect detection, especially for bicolour varieties, is a difficult task using standard image acquisition devices (colour or NIR cameras). On the other hand, economical and practical considerations must be taken into account in the development of automatic apple sorting machines. Using MIR cameras or X-ray systems, which are expensive devices, to address one particular problem such as stem-ends/calyxes or bruises could prove not to be cost effective. Hyper-spectral imaging systems provide a large amount of data which is very time consuming to acquire and to process. The aim of this research was thus to propose an image acquisition and processing method enhancing the detection of a wide range of defects on apples and having the potential of being applied industrially. 'Jonagold' apple was studied because it is a bicolour variety presenting a high variability in the skin colour. Due to this variability, a lot of defects were poorly contrasted and therefore difficult to detect.

2. Materials and methods

2.1. Image acquisition device

On the basis of the study carried out by Kleynen, Leemans, and Destain (2003) about the selection of band-pass filters for 'Jonagold' apple sorting, a four band multi-spectral image acquisition device was set up (Fig. 1). It was made of a 'MultiSpec Agro-Imager^{TM}, (Optical Insights LCC, USA) including four interference band-pass filters and coupled to a high resolution (1280×1024 pixels) monochrome digital

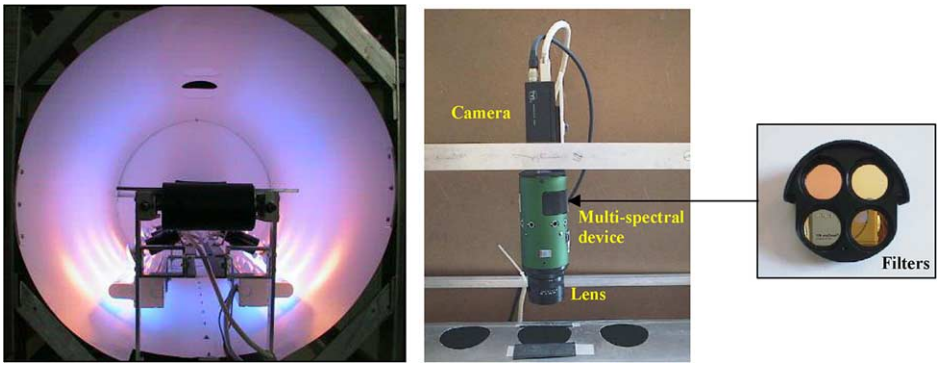

Fig. 1. Lighting tunnel and multi-spectral image acquisition device.

camera (CV-M4CL, JAI sa, Denmark). The used filters were centred at 450, 500, 750 and 800 nm and had, respectively, a bandwidth (FWHM) of 80, 40, 80 and 50 nm (Melles Griot bv, The Netherlands). The 'Multi-Spec Agro-Imager™, is an optical device that projects on a single array CCD sensor four images of the same object corresponding to four different spectral bands using four removable standard interference filters. It was equipped with a 'Cinegon 1.8/4.8' lens (Schneider Optics Inc., USA). Images were acquired with a grey level resolution of 8 bits per pixel using a Camera Link frame grabber (GRABLINK™ Value, Euresys sa, Belgium). In order to provide sufficient light in each of the four wavelength bands, a lighting tunnel including two different light sources was designed. The selected lighting sources consisted of two Philips 'TL-D 18 W/18' fluorescent tubes emitting in the spectral band of the blue colour and ten 30 W incandescent spots emitting in the visible and near-infrared spectra. They were placed below the level of the fruit to avoid direct illumination leading to specular reflection. The inner surface of the tunnel was painted in flat white to provide a uniform diffuse light. The optical resolution (ability to distinguish object detail) of the acquired images was evaluated by imaging frequency targets. The frequency targets consisted of a succession of black lines spaced from a distance equal to their width. Four line widths were considered: 0.25, 0.50, 0.75 and 1.00 mm. The resolution of the imaging system was then defined by the smallest width under which black lines start blending together. Blending was estimated by computing the magnitude of the Fourier transform coefficients of an average image line profile measured perpendicularly to the black line direction. An average image line profile consisted of the mean values of 10 profiles. For a given frequency target, the magnitude of the Fourier transform coefficient corresponding to the frequency of the black lines was a measurement of the contrast between the light and dark lines expressed in terms of grey levels. We considered that above a magnitude of 8 grey levels, the contrast was sufficient. Measurements showed that the minimum resolution was 0.75 mm for the four spectral bands. However, the contrast varied with the spectral band. It was about 10, 55, 13 and 22 grey levels, respectively, for the filter centred at 450, 500, 750 and 800 nm.

2.2. Image calibration

One multi-spectral image acquired with the above described system was therefore formed of four sub-images corresponding each to one filter. Since the pixel's coordinates of the four sub-images did not match perfectly, sub-image alignment was necessary before further image analyses. To identify the centres of the four sub-images, the pattern matching function ('EasyMatch') of the 'EasyAccess' software (Euresys sa, Belgium) was used. This function computes also the x/y scale factors and the orientation angle existing between the pattern and the identified objects. The used pattern was the sub-image corresponding to the filter centred at 800 nm. Table 1 presents the geometrical differences between the 800 nm sub-image and the other spectral components. Inverse geometrical transforms were then applied on each sub-image.

Since vignetting was also observed on the multi-spectral images (sub-image borders were darker than the centre), a 'flat field correction' was applied on each of the sub-images. This process corrects uneven illumination over the field of the array CCD and the electronic offset due to the inherent structure of the CCD (dark current). Flat fielding required the acquisition of two calibration images: a bias image (BI) and a flat field image (FFI). BI was obtained by recording an image

Table 1
Geometrical differences between the 800 nm sub-image and the other spectral components

Sub-image (nm)	Angle (°)	Scale x (%)	Scale y (%)
450	0.291	99.31	99.11
500	0.291	100	100
750	0	100	100

with the light source turned off. FFI was obtained by imaging a uniform pattern with a colour representative of the 'Jonagold' apples in the specific lighting conditions. This was done with a pattern having the following $L^*a^*b^*$ colour: $L^* = 61$, $a^* = -38$ and $b^* = 43$. Corrected image (CI) was then defined according to the following equation:

$$\mathrm{CI} = \frac{(\mathrm{RI} - \mathrm{BI}) \cdot \mathrm{MFFI}}{\mathrm{FFI} - \mathrm{BI}}$$

where RI is the raw uncorrected image and MFFI is the average pixel value of FFI.

2.3. Apple image database

Two hundred and eighty multi-spectral images of sound 'Jonagold' apples were acquired tending to cover the whole colour variability of this bicolour apple variety. On the other hand, 246 images of a wide range of defects were taken. Those defects consisted of scald, hail damage (with and without skin perforation), limb rubs, russets, scar tissue, frost damage, rot, visible flesh damage and recent bruises (between 1 h and 2 h old). Bruises were made by dropping the fruit from a 30 cm height onto a steel plate mounted on a 12 kg mass. Defects were grouped into four categories according to their severity and size: slight defects (e.g. small russet), more serious defects (e.g. scar tissue), defects leading to the rejection of the fruit (e.g. rot) and recent bruises. In order to evaluate the influence of stem-ends and calyxes on the defect detection, 292 images of stem-ends and calyxes were recorded with various orientations according to the optical axis of the camera. Fig. 2 presents an example of multi-spectral image. It can be noticed that the 500 nm spectral band (corresponding to the green visible spectrum) offered the best contrast between the blush (low grey levels) and the ground colour (high grey levels) while the 750 and 800 nm bands were not sensitive to the natural colour variations of the fruit and offered a good contrast between the defect and the sound tissue. According to the observation of Lammertyn, Peirs, De Baerdemaeker, and Nicolai (2000), the light penetration depth was the highest in these two spectral bands. They were therefore well suited to detect internal tissue damage like hail damage, bruises, etc. The 450 nm spectral band brought more significant information to identify slight surface defects like russet.

2.4. Stem-end and calyx recognition

Since stem-ends and calyxes appear as defects when processing the images, they must be recognised prior to any further data analysis. The recognition was based on a similarity template matching algorithm provided with the 'Intel Integrated Performance Primitives 3.0' library (Intel Corporation, USA) and implemented in C++. Given a source image and a stem-end/calyx template image, the algorithm returned a resulting image where the pixel value characterise the similarity between each point of the source image and the stem-end/calyx template. The similarity at location (x, y) in the source image was estimated with the correlation coefficient and was calculated as following:

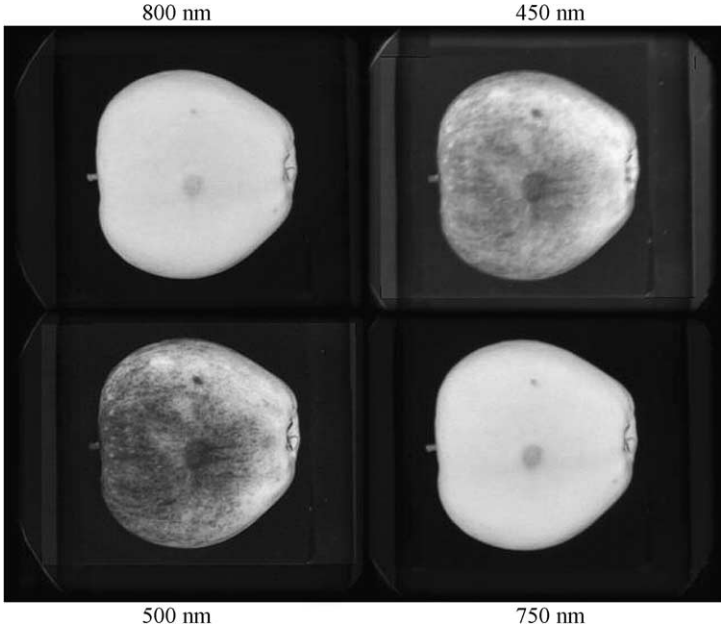

Fig. 2. Example of a multi-spectral image of a hail damage (in the centre of the view).

$$r(x,y)=\frac{\sum_{y'=0}^{h-1}\sum_{x'=0}^{w-1}\left[(T(x',y')-\overline{T})\cdot(I(x+x',y+y')-\overline{I}(x,y))\right]}{\sqrt{\sum_{x'=0}^{w-1}\sum_{y'=0}^{h-1}(T(x',y')-\overline{T})^2\cdot\sum_{x'=0}^{w-1}\sum_{y'=0}^{h-1}(I(x+x',y+y')-\overline{I}(x,y))^2}}$$

where $r(x,y)$ is the value of the correlation coefficient at location (x,y) in the source image; I is the source image; T is the template image with the dimensions $h\times w$ pixels; $\overline{T}$ is the average of the pixel values in the template and $\overline{I}(x,y)$ is the average value of the pixel values in the current window $(h\times w)$ of the source image.

The correlation coefficient is a parameter varying between 0 when there is no relation between the template and the source image and 1 when both match perfectly. The resulting correlation image was then thresholded at a level of 0.80. If no object was detected in the thresholded image, the current view of the apple did not present any stem-end or calyx. Otherwise, the gravity centre of the detected object indicated the centre of the template.

Since this method could only be applied on single channel images, it was chosen to work with the 800 nm spectral band. Indeed, that wavelength band was not influenced by natural variations of the skin colour and offered the best contrast between the stem-ends/calyxes and the rest of the fruit. The template used was an average image of 5 stem-ends and 5 calyxes. Fig. 3 presents, as an example, the result of the correlation template matching method for the detection of a calyx.

2.5. Fruit segmentation into sound and defective tissue

Each pixel of the fruit was classified into the 'sound' or 'defect' class according to the values of its spectral components. On the basis of the Bayes' theorem (Leemans, Magein, & Destain, 1999), the probability of a given pixel to belong to the sound class was determined by the following equation:

$$P(\text{sound}/x)=\frac{P(x/\text{sound})\cdot P(\text{sound})}{P(x)}$$

with

$$P(x)=P(\text{sound})\cdot P(x/\text{sound})+P(\text{defect})\cdot P(x/\text{defect})$$

where x is the vector of the spectral components; $P(\text{sound}/x)$ is the a posteriori probability for a pixel characterised by the x vector to belong to the sound class; $P(x/\text{sound})$ is the probability for a pixel belonging to the sound class to be characterised by the x vector; $P(\text{sound})$ is the a priori probability to observe a pixel belonging to the sound class; $P(x)$ is the probability to observe a pixel characterised by the x vector when all classes are blended; $P(\text{defect})$ is the a priori probability to observe a pixel belonging to the defect class and $P(x/\text{defect})$ is the probability for a pixel belonging to the defect class to be characterised by the x vector.

A given pixel was therefore allocated to the sound class if the $P(\text{sound}/x)$ probability was greater than 0.5, otherwise it was allocated to the defect class.

Since only two classes were taken into account, $P(\text{sound}/x)=1-P(\text{defect}/x)$. In order to prevent an over- or under-segmentation of the defect, it was assumed that the a priori probability to observe a pixel belonging to the sound class was equal to the a priori probability to observe a pixel belonging to the defect class. Therefore:

$$P(\text{sound})=P(\text{defect})=0.5$$

$$P(x)=0.5\cdot P(x/\text{sound})+0.5\cdot P(x/\text{defect})$$

$$P(\text{sound}/x)=\frac{P(x/\text{sound})}{P(x/\text{sound})+P(x/\text{defect})}$$

The computation of the $P(\text{sound}/x)$ probability required at last to estimate two parameters $P(x/\text{sound})$ and $P(x/\text{defect})$. These two parameters were estimated with the relative frequency distributions of the spectral components of the sound and defective tissue which tend to the corresponding probability distribution when the sample size grows.

The frequency distribution of the sound tissue was established on the basis of an automatic selection of pixels belonging to sound fruits. This was done by first separating the fruit from the background by simply thresholding the sub-image corresponding to 800 nm spectral band. A morphological erosion filter was then applied to remove the pixels belonging to the borders of the fruit which appeared darker due to the spherical

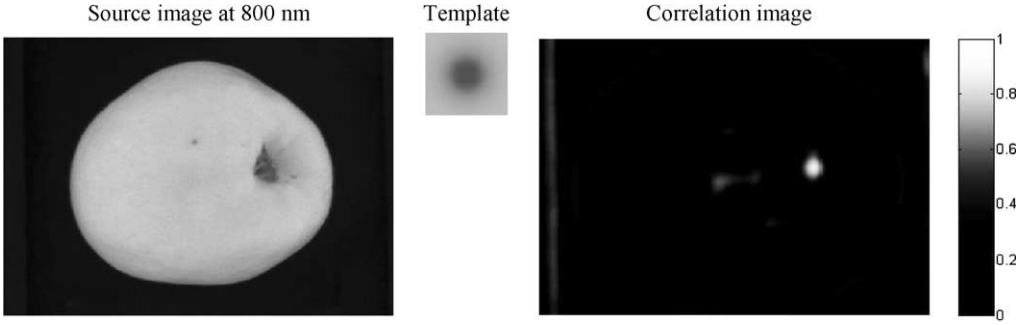

Fig. 3. Example of the correlation template matching method applied for the detection of a calyx.

shape of the apples. The pixels of the eroded image of the fruit were then used to compute the frequency distribution. With regard to the frequency distribution of the defects, a manual selection of defective tissue pixels was needed.

Since each of the four spectral components was coded on 8 bits (256 grey levels), the calculation of the 4 dimension frequency distributions needed at least a memory storage of 16 gigabytes (256^4 combinations $\times$ 4 memory bytes for each combination). Consequently, due to technical limitations, only distributions of three spectral components were computed (these ones requiring only 65 Mb of memory storage). Since Kleynen et al. (2003) showed that the 500 nm spectral component did not give any significant information for the discrimination of the defects and sound tissue (it was only interesting to quantify the ratio between the blush and ground colour), this component was not taken into account for the computation of the frequency distributions.

Fig. 4 presents the projections of the frequency distributions of the sound and defective tissue onto the planes defined by the 450/750 nm and 750/800 nm spectral components. It can be noticed that the distribution of the sound tissue obeyed a Gaussian multi-variate model which presented a high variability in the blue visible spectrum (spectral component of 450 nm) due to the natural variations in the skin colour. The 750 and 800 nm spectral components were clearly less influenced by

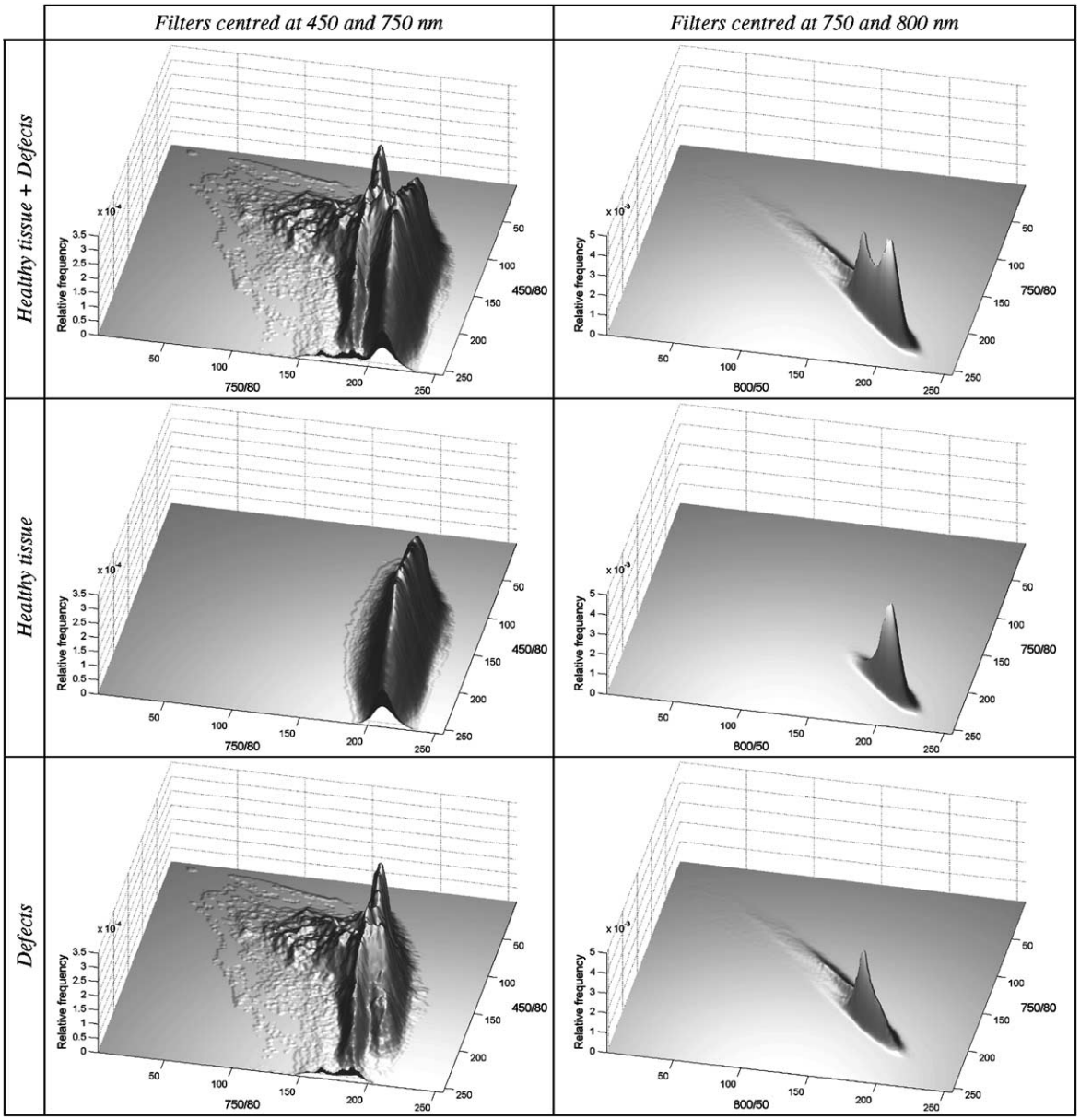

Fig. 4. Projections of the frequency distributions of the sound and defective tissue onto the planes defined by the spectral components corresponding to the filters centred at 450/750 nm and 750/800 nm.

those natural variations. In these two last wavelength bands, most of the defect's pixels were generally darker than the sound tissue's pixels. In all wavelength bands, defect's pixels covered a wide range of intensities. Moreover, the distribution of the defects could not be approximated by a given model which demonstrated the interest to use the relative frequency distributions instead of parametric models. On the other hand, even if the 750 and 800 nm spectral components were highly correlated, both were necessary to discriminate some defects with a colour very close to the sound tissue (see part 3).

Based on the two 3D frequency distributions of the sound and defective tissue, the $P(\text{sound}/x)$ probabilities were computed once 'off-line' and written in a look-up table. The 'on-line' segmentation consisted finally in comparison of the value of the look-up table corresponding to the 450, 750 and 800 nm spectral components to the value of 0.5.

2.6. Fruit classification

In order to estimate the precision of the defect detection, classification tests of fruits into the 'sound' or 'defective' class were performed. Once the fruit was segmented into sound and defective tissue, the following discriminant features were computed on both tissue classes: the mean, the median and the standard deviation values of the 450, 750 and 800 nm spectral components. Those spectral features plus the ratio of tissue segmented as defective were then introduced in a linear discriminant analysis procedure. Correct classification rates of sound and defective apples were finally estimated by cross-validation.

3. Results and discussion

The correlation pattern matching method allowed to recognise 91% of the stem-ends and 92% of the calyxes. As shown in Fig. 5 line 1, stem-ends and calyxes not recognised presented a bad orientation according to the optical axis of the camera. This kind of error could therefore be solved by taking multiple views of the fruit and registering them geometrically as presented by Leemans and Destain (2004). With regard to defects, 17% were identified as stem-end/calyx. They were generally very dark with a circular shape and leading in most of the cases to the rejection of the fruit (Fig. 5 line 2). If multiple views of the fruit were acquired, more than two stem-ends/calyxes should be detected on apples with such defects. Since sound apples presents only one stem-end and one calyx, the detection of more than two stem-ends/calyxes on a fruit should lead to the rejection of this one.

The results of the cross-validation of the fruit classification into sound and defective classes showed that 94.3% and 84.6% of the sound and defective apples were, respectively, well classified. Fig. 6 shows examples of defective fruits (russet and recent bruise) correctly classified thanks to the dedicated multi-spectral vision system. Indeed, those defects were particularly difficult to detect with conventional imaging system. Further analyses of the classification errors revealed that most of the misclassified sound fruits were confused with fruits having slight defects. A small part was classified among the fruits with recent bruises. With regard to the defective fruits, Table 2 presents the correct classification rates according to the four defect categories. No rejected fruit and only 2% of the recent bruises were

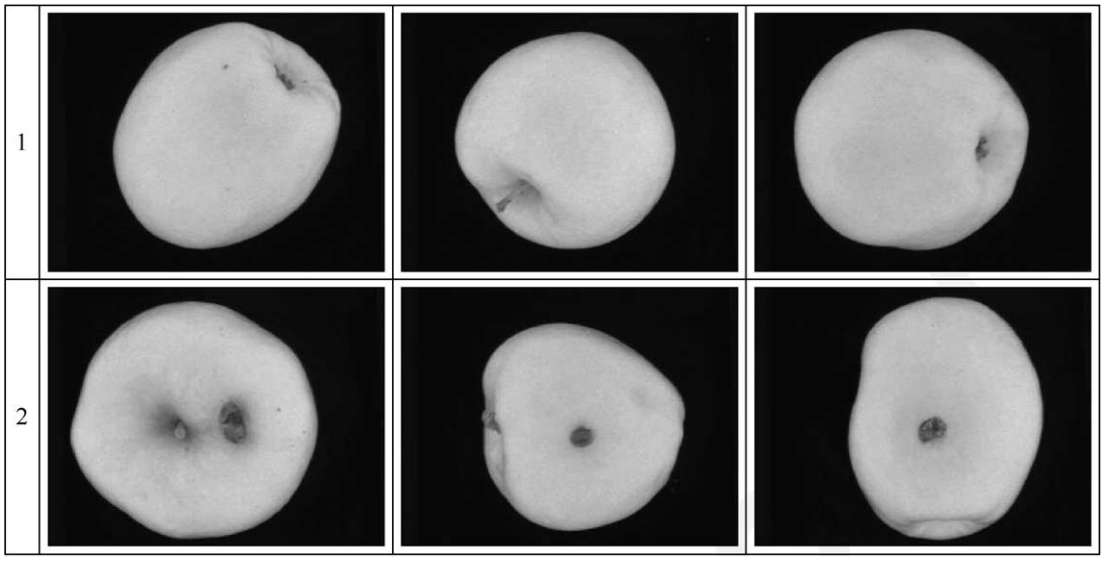

Fig. 5. Examples of errors made with the correlation pattern matching method (800 nm spectral band). (1) Stem-ends or calyxes not recognised. (2) Defects confused with the stem-ends/calyxes.

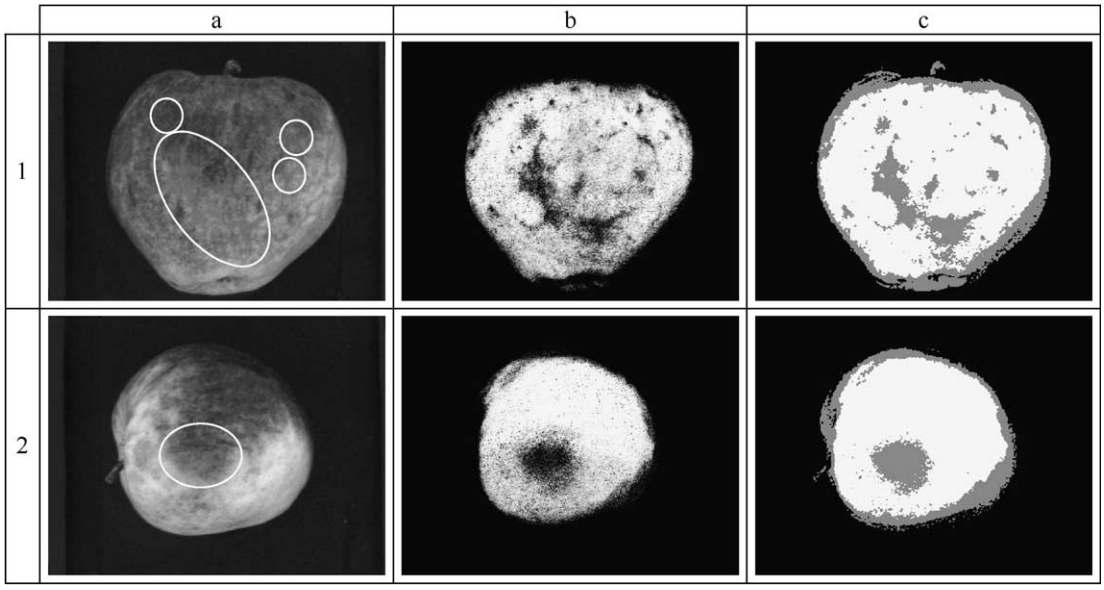

Fig. 6. Examples of defective fruits correctly classified into the defective class. (1) Russet. (2) Recent bruise. (a) Original image corresponding to the 500 nm spectral band and offering the best visual contrast (defects are surrounded in white). (b) Image of the $P(\text{sound}/x)$ probabilities (grey level refers to the probability value, black = 0, white = 1). (c) Result of the segmentation process (threshold value = 0.5, white = sound tissue, grey = defect).

Table 2
Correct classification rates of the defect categories

Defect class	Correct %
Rejected	100
Recent bruises	98.2
Serious	94.5
Slight	55
Global rate	84.6

misclassified into the sound class. About 6% of the serious defects were classified into the sound fruits. It must be noticed that this kind of defects does not lead to the rejection of the fruit but relegates it to a lower quality category. The impact of those errors was therefore relatively less serious than classifying a rotten or flesh damaged apple into the sound fruits. Regarding slight defects, 45% of the defective apples were still confused

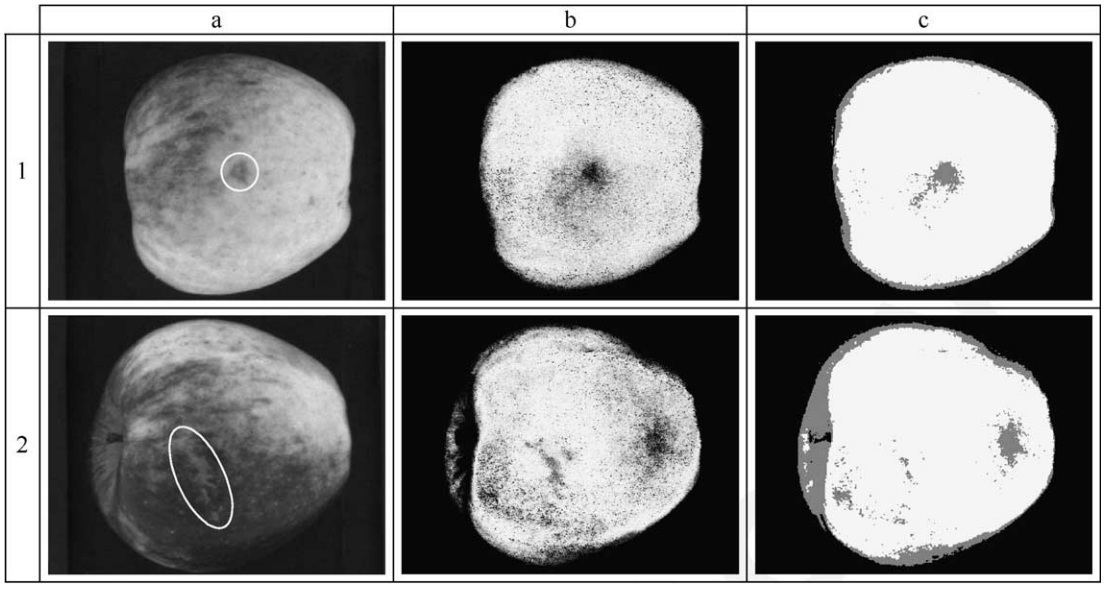

Fig. 7. Examples of defective fruits misclassified into the sound class. (1) Small scald correctly segmented. (2) Russet poorly segmented. (a) Original image corresponding to the 500 nm spectral band and offering the best visual contrast (defects are surrounded in white). (b) Image of the $P(\text{sound}/x)$ probabilities (grey level refers to the probability value, black = 0, white = 1). (c) Result of the segmentation process (threshold value = 0.5, white = sound tissue, grey = defect).

with the sound fruits. As presented in Fig. 7, the errors consisted mainly of defects well segmented but with a small area (line 1) or of defects having a colour similar to the sound tissue and therefore poorly segmented (line 2). Nevertheless, those defects were minor and acceptable according to the quality tolerances defined by the European standard. Considering that a raw batch of apples contains actually about 90% of sound fruits, the ratio of defective fruits misclassified into the sound class dropped to 1.9% which fits the 5% quality tolerance of the 'extra' class.

The complete computing time including the stem-end/calyx recognition, the defect segmentation and the fruit classification implemented in a C++ program was about 30 ms with a 'Pentium III 866 MHz' processor and using the 'Intel Integrated Performance Primitives 3.0' library. Considering multiple views per fruit and with up to date processors, this computing time is totally compatible with the industrial sorting speeds.

Since it was observed (Fig. 4) that the 750 and 850 nm spectral components were highly correlated, the interest to use them simultaneously was evaluated by making a fruit classification test taking into account only the spectral discriminant attributes related to the 450 and 750 nm spectral components. It was then observed that the correct classification rate of the defective fruits dropped from 84.6% to 80.1%. This diminution came from an increase in the errors made on the slight defects like russet and hail damage.

Finally, to confirm that the 500 nm spectral component was not significant for discriminating sound apples from defective ones, a classification test taking into account the information provided by the 4 spectral components was performed. In that case, the misclassification rate of the defective apples increased slightly due to a loss of significant information introduced by the 500 nm spectral component which was highly correlated to the natural variations of the skin colour. The 450, 750 and 800 nm spectral components were therefore sufficient and well suited to sort 'Jonagold' apples.

4. Conclusion

The global methodology consisting in selecting a reduced number of spectral bands and implementing the corresponding filters in a multi-spectral image acquisition device was found appropriate for defect detection on apples. The most efficient wavelength bands were centred at 450, 750 and 800 nm. The 450 nm spectral band brought significant information to identify slight surface defects like russet while the 750 and 800 nm bands offered a good contrast between the defect and the sound tissue and were well suited to detect internal tissue damage like hail damage, bruises, etc. A Bayesian classification procedure was successfully used to segment these defects.

The proposed methodology has the potential for being used in apple sorting machines. Indeed, the selection of the most efficient wavelength bands can be done once 'off-line' and consequently, the 'on-line' process consisting in image acquisition and analyses may occur at acceptable speeds. The efficiency of the method was demonstrated on a bicolour apple variety presenting a high colour variability. The procedure has therefore the potential for being extended to other varieties.

Acknowledgements

This research is funded by the General Directorate of Technology, Research and Energy of the Walloon Region (Belgium). Convention no. 9813783.

References

Anonymous (2001). Commission Regulation (EC) No 1619/2001 of 6 August 2001 laying down the marketing standard for apples and pears. *Official Journal L 215*, 09/08/2001, 0003-0016.

Cheng, X., Tao, Y., Chen, Y. R., & Luo, Y. (2003). NIR/MIR dual-sensor machine vision system for online apple stem-end/calyx recognition. *Transactions of the ASAE, 46*(2), 551–558.

Kleynen, O., Leemans, V., & Destain, M. F. (2003). Selection of the most efficient wavelength bands for 'Jonagold' apple sorting. *Postharvest Biology and Technology, 30*, 221–232.

Lammertyn, J., Peirs, A., De Baerdemaeker, J., & Nicolai, B. (2000). Ligth penetration properties of NIR radiation in fruit with respect to non-destructive quality assessment. *Postharvest Biology and Technology, 18*, 121–132.

Leemans, V., & Destain, M. F. (2004). A real-time grading method of apple based on features extracted from defects. *Journal of Food Engineering, 61*, 83–89.

Leemans, V., Magein, H., & Destain, M. F. (1999). Defect segmentation on 'Jonagold' apples using colour vision and a Bayesian classification method. *Computers and Electronics in Agriculture, 23*, 43–53.

Li, Q. Z., Wang, M. H., & Gu, W. K. (2002). Computer vision based system for apple surface defect detection. *Computers and Electronics in Agriculture, 36*(2–3), 215–223.

Mehl, P. M., Chen, Y. R., Kim, M. S., & Chan, D. E. (2004). Development of hyperspectral imaging technique for the detection of apple surface defects and contaminations. *Journal of Food Engineering, 61*, 67–81.

Shahin, M. A., Tollner, E. W., McClendon, R. W., & Arabnia, H. R. (2002). Apple classification based on surface bruises using image processing and neural networks. *Transactions of the ASAE, 45*(5), 1619–1627.

Wen, Z., & Tao, Y. (1999). Building a rule-based machine-vision system for defect inspection on apple sorting and packing lines. *Expert Systems with Applications, 16*, 307–313.